Available online at www.sciencedirect.com
SCIENCE DIRECT®

Journal of the European Ceramic Society 23 (2003) 1697–1704

www.elsevier.com/locate/jeurceramsoc

Influence of temperature, ripening time and calcination on the morphology and crystallinity of hydroxyapatite nanoparticles

Y.X. Pang, X. Bao*

Institute of Polymer Technology and Materials Engineering, Loughborough University, Loughborough, Leicestershire LE11 3TU, UK

Received 30 March 2002; received in revised form 22 October 2002; accepted 28 October 2002

Abstract

Nano-sized hydroxyapatite (HA) particles were prepared by chemical precipitation through aqueous solutions of calcium chloride and ammonium hydrogenphosphate. The influence of temperature, ripening time and calcination on the crystallinity and morphology of the HA nanoparticles were investigated. It was found that the crystallinity and crystallite size increased with the increase of synthetic temperature and ripening time. XRD and TEM results showed that the morphology change of HA nanoparticles was related to their crystallinity. High crystallinity of HA led to regular shape and smooth surface of the nanoparticles. The crystallinity of HA powders increased greatly after calcination at 650 °C for 6 h but the change of the crystallite size after calcination was dependent on the crystallinity and crystallite size of "as prepared" HA nanoparticles.

Keywords: Apatite; Crystallinity; Hydroxyapatite nanoparticles; Powders—chemical preparation; Precipitation

1. Introduction

The synthesis of HA has been a major subject for chemists and materialists over the years since it is one of the most attractive and important bioceramics.[1] The synthetic HA has excellent biocompatibility and promising bioactivity due to its resemble composition and structure to bone and tooth minerals.[2–4] Although the chemical synthesis of HA came back to several decades ago, the synthetic methodology has been developing over the years in order to satisfy the requirements for various biomedical applications. There are various routes available for HA preparation. These include mechanochemical synthesis,[5] combustion preparation,[6] and various techniques of wet chemistry, such as direct precipitation from aqueous solutions,[7,8] electrochemical deposition,[9] sol-gel procedures,[10,11] hydrothermal synthesis,[12,13] and emulsion or microemulsion routes.[14,15] Among them, chemical precipitation from aqueous solutions provides a versatile and economic route. The resulting suspension can be used as surface coatings,[16,17] as bulk materials after drying,[18] or to form HA powders with controlled morphology by atomisation or spray drying,[19,20] etc. However, the microstructure and property of the resulting HA suspensions vary greatly with synthetic variables. The pH value of the reaction system is crucial for HA formation[21] and the synthetic temperature,[22] purity of starting materials[23] and mixing procedure of reactants[8] are also of great importance for HA formation.

The properties of synthesised HA powder, such as crystallinity, morphology and particle size will affect the effectiveness of the powder in its application. It was reported that small changes in particle size and morphology in the HA/polyethylene composites had significantly effects on the mechanical properties of the composite.[24]

Although the influence of temperature on crystallinity of precipitated HA was mentioned in several reports,[22,25] no details were presented. The objective of this work is to study the effects of temperature, ripening time and calcination upon the particle morphology and crystallinity of the HA nanoparticles.

* Corresponding author. Tel.: +44-1509-223150; fax: +44-1509-223949.
E-mail address: x.bao@lboro.ac.uk (X. Bao).

0955-2219/02/$ - see front matter © 2003 Elsevier Science Ltd. All rights reserved.
PII: S0955-2219(02)00413-2

2. Experimental details

2.1. Synthesis of HA

Nano-sized HA particles were prepared by chemical precipitation through aqueous solutions of the reactants. Calcium chloride and ammonium hydrogenphosphate (both supplied by Aldrich) were first dissolved in deionised water to form 0.5 and 0.3 M aqueous solutions, respectively. Equal amounts of these two aqueous solutions were separately pre-heated to the synthetic temperature and then mixed under vigorous stirring. Meanwhile, ammonium hydroxide (Fisher Scientific UK) was added immediately to adjust the reaction mixture to pH 10. The pH value was kept constant throughout the experiment. After ripening for a specified period of time, the precipitates were recovered by centrifuge and then washed with water. At least five cycles of washing and centrifuging were required to ensure complete removal of the by-product, ammonium chloride.

For the HA prepared at various temperatures from 15 to 99 °C (refluxing), the ripening time was kept for 24 h. For those with various ripening times from 1 to 96 h, a set of samples was obtained from the same batch of the reaction by sampling at time intervals, so that minimises the experimental error.

The calcination of HA powders synthesised under different temperatures and ripening times was carried out by first drying the samples at 70 °C for 24 h in a vacuum oven and then calcining at 650 °C for 6 h at the ramp rate of 5.0 °C/min in a tube furnace.

2.2. Characterisation

The phase composition and crystallinity of the "as prepared" and calcined HA nanoparticles were analysed by X-ray diffraction (XRD) using a Brüker AXS, D8 Advance Diffractometer with CuK_α radiation $\lambda = 0.15406$ nm at 40 kv and 30 mA. Data were collected over the 2θ range 20–45° with a step size of 0.014° and a count time of 0.5 s.

The morphology study performed on the "as prepared" HA nanoparticles was done using a transmission electron microscope (TEM) (JEM 100CX, Jeol, Japan).

FTIR spectra were obtained using a Mattson 3000 FTIR spectrometer (Unicam Ltd., England). The spectra were recorded from 600 to 4000 wavenumbers at 4 cm^{-1} resolution averaging 64 scans. The HA powders used for FTIR measurement were dried in a vacuum oven at 70 °C for 2 weeks. Small amount of HA powders were blended with KBr and then pressed into discs for the measurement.

Thermogravimetry and differential thermal analyses (TG–DTA) were carried out on a 2690 Simultaneous TG–DTA analyser (TA instruments). The measurements were conducted from ambient temperature to 750 °C at heating rate of 5.0 °C/min under air atmosphere. The sample size is 20 mg and the samples were dried in a vacuum oven at 70 °C for 2 weeks before measurement.

3. Results and discussion

3.1. Effect of temperature

The XRD spectra of HA powders prepared at different synthetic temperatures are shown in Fig. 1. All samples resulted in diffraction peaks that only corresponded to the standard for hydroxyapatite.[26] Broad diffraction peaks were observed for the HA powders synthesised at low temperature (15 °C). With the increase in synthetic temperature these diffraction peaks become sharp, indicating the increase in crystallinity of HA powders synthesised.

The fraction of crystalline phase (X_c) in the HA powders can be evaluated by the following equation:[25]

$$X_c = 1 - \left(V_{112/300}/I_{300}\right) \quad (1)$$

where I_{300} is the intensity of (300) diffraction peak and $V_{112/300}$ is the intensity of the hollow between (112) and (300) diffraction peaks of HA. The evaluated degrees of crystallinity for these samples are given in the Table 1. The crystallinity increased from 0.03 to 0.53 for the HA powders prepared at 15 and 99 °C (refluxing), respectively, which indicated a strong synthetic temperature-dependence of the crystallinity of the HA prepared. It was noticed that the increase of the crystallinity with temperature was not linear. There was no significant change in crystallinity when the synthetic temperature was lower than 70 °C. However, sharp increases in the crystallinity were observed when the synthetic temperatures were over 70 °C, as the crystalline activation energy of the HA was overcome at that temperature. Bouyer et al. reported a similar phenomenon.[22] They

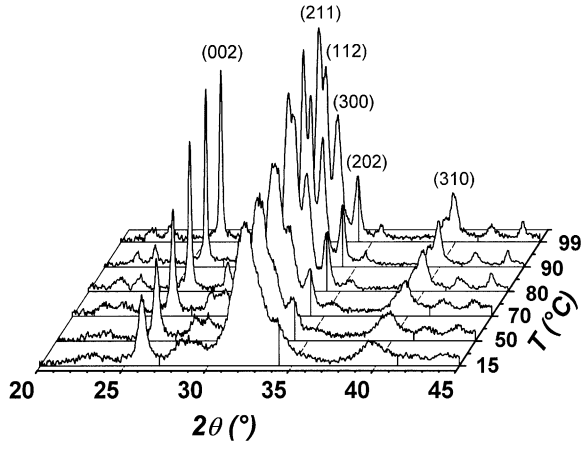

Fig. 1. XRD spectra of the HA nanoparticles synthesised at various temperatures with ripening time for 24 h.

Table 1
The effect of synthetic temperature on the crystallinity and crystallite size of HA nanocrystals before and after calcination at 650 °C for 6 h

Temperature (°C)	Crystallinity X_c (%)		Crystallite size X_s (nm)	
	Before calcination	After calcination	Before calcination	After calcination
15	0.03	0.39	20.8	35.1
50	0.06	0.58	27.8	37.3
70	0.10	0.63	34.9	42.7
80	0.32	0.65	45.9	44.0
90	0.48	0.71	50.0	46.5
99	0.53	0.72	52.7	47.4

found that 60 °C was a transition temperature. Below that temperature the HA crystals are monocrystalline, while above this temperature the HA crystals become multicrystalline. The sharp increase in the crystallinity of HA synthesised above 70 °C in this study is also due to the formation of multicrystalline HA crystals.

The peak broadening of XRD reflection can be used to estimate the crystallite size in a direction perpendicular to the crystallographic plane based on Scherrer's formula as follows:[27]

$$X_s = 0.9\lambda/(\mathrm{FWHM} \times \cos\theta) \quad (2)$$

where X_s is the crystallite size [nm]; λ the wavelength of monochromatic X-ray beam [nm] ($\lambda = 0.15406$ nm for CuK_α radiation); FWHM the full width at half maximum for the diffraction peak under consideration [rad]; and θ the diffraction angle [°]. The diffraction peak at $2\theta = 26.04°$ was chosen for calculation of the crystallite size since it is sharper and isolated from others. This peak assigns to (002) Miller's plane family and shows the crystal growth along the c-axis of the HA crystalline structure.[28] The calculated X_s for the HA powders synthesised at different temperatures based on this diffraction peak using Scherrer's formula is also listed in Table 1. The crystallite sizes of the "as prepared" HA powders were smaller than 50 nm and an increase in crystallite size of the HA powders with the increase of synthetic temperature was observed, i.e. the higher of the synthetic temperature, the larger of the crystallite size of the HA nanocrystals formed.

The morphologies of the HA particles prepared at different synthetic temperatures are shown in Fig. 2. All the HA samples showed nano-sized needle-like morphology with particle width ranged from 20 to 40 nm and the length from 100 to 300 nm, respectively. However, the appearance of these nanoparticles was quite different from each other. The particles synthesised at low temperatures were a bit thinner and longer, with

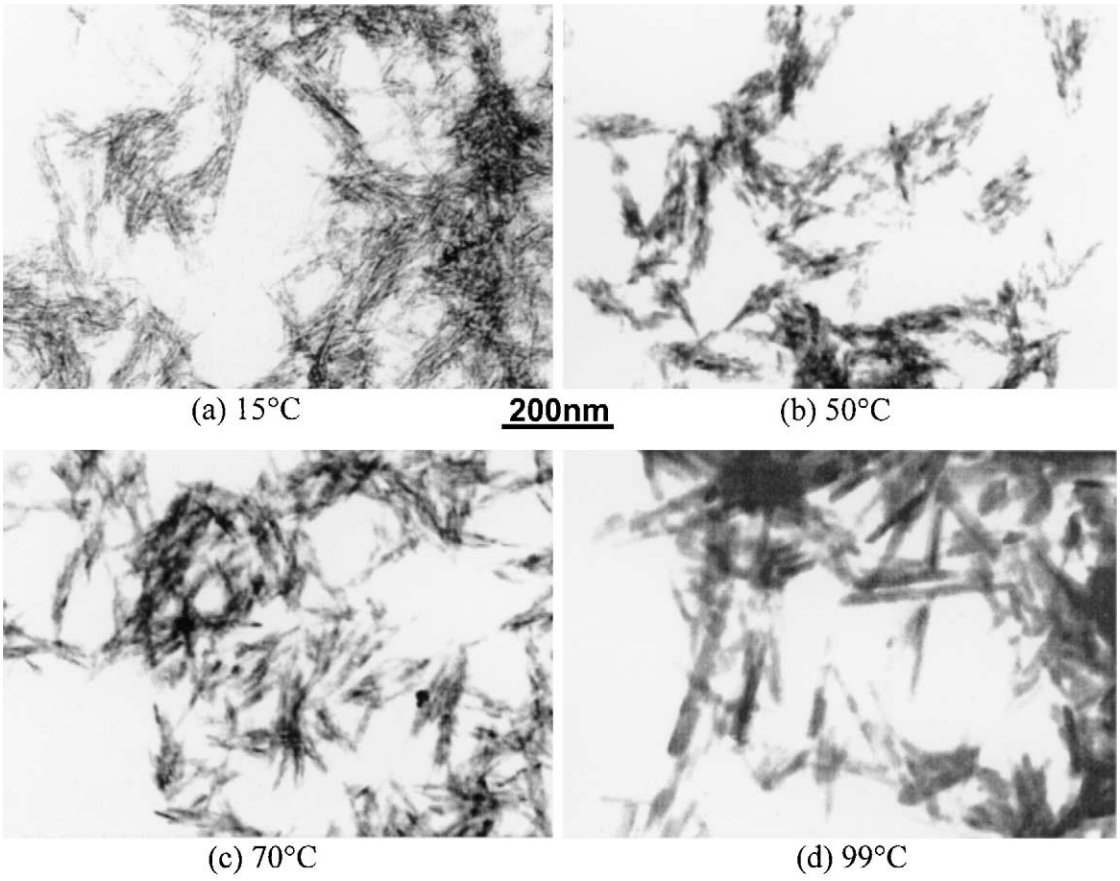

Fig. 2. TEM micrographs of the HA nanoparticles synthesised at various temperatures.

more irregular and less clear contours. Also the particles showed high tendency to agglomerate. On the other hand, for the samples prepared at higher temperatures, the particles were slightly thicker and shorter, with more regular shape and clearer contours and less aggregation. The change from irregular to regular particle morphology with the increase in synthetic temperature was corresponding to the increase of the crystallinity of the HA nanocrystals, that is, more regular shape of the particles was observed when the powders had higher crystallinity.

3.2. Effect of ripening time

Ripening time is another important factor to influence the crystallinity and the morphology of the HA nanoparticles synthesised. Fig. 3 shows the XRD diffraction patterns of the HA prepared at 80 °C with various ripening times. The increase of crystallinity with the increase of the ripening time was observed clearly by the sharpening of the diffraction peaks of the HA powders. The crystallinity and crystallite size calculated by Eqs. (1) and (2) as a function of ripening time are given in Table 2. Both the crystallinity and crystallite size of the HA powders increased very rapidly at the early ripening stages and gradually levels off as ripening lasted. Similar results were obtained when the synthetic temperature was raised to 99 °C (refluxing). The absolute values of crystallinity and crystallite size, however, were higher for the HA powders prepared at 99 °C (Table 3) than at 80 °C.

Table 2
The X_c and X_s values for the HA powders prepared at 80 °C as a function of ripening time

Ripening time (h)	Crystallinity X_c (%)		Crystallite size X_s (nm)	
	Before calcination	After calcination	Before calcination	After calcination
1	0.13	0.45	34.2	36.3
3	0.15	0.49	38.9	39.4
6	0.21	0.50	39.4	40.9
12	0.27	0.59	43.0	42.3
24	0.32	0.62	45.9	43.3
96	0.44	0.71	48.5	44.8

Table 3
The X_c and X_s values for the HA powders prepared at 99 °C as a function of ripening time

Ripening time (h)	Crystallinity X_c (%)		Crystallite X_s (nm)	
	Before calcination	After calcination	Before calcination	After calcination
1	0.34	0.69	46.1	45.5
3	0.46	0.70	49.4	48.1
6	0.50	0.70	51.7	48.4
12	0.50	0.71	52.5	50.2
24	0.53	0.72	53.9	51.3
96	0.64	0.75	58.3	55.7

This profile of crystallinity increase with ripening time was also proved by FTIR analysis. Fig. 4 shows the FTIR spectra of HA powders synthesised at 80 °C with ripening time for 1 h ($X_c = 0.13$) and 96 h ($X_c = 0.44$). The spectrum for the calcined powder is also displayed in this figure. The characteristic bands for HA are exhibited in all the three spectra: 900–1200 cm^{-1} for phosphate stretching, 602 cm^{-1} for phosphate bending, 632 and 3571 cm^{-1} for hydroxyl vibrations.[9,15,29] The intensities of these two hydroxyl absorption bands and the band at 940 cm^{-1} for phosphate can be used as an indication of the HA crystallinity.[15] It is seen that the intensities of these three bands increase with the ripening time, by comparison of spectra (a) and (b) in Fig. 4. This result is consistent with the above XRD results (Fig. 3). In addition, the broad band at 2500–3700 cm^{-1}, which is a reflection of the combined water in HA

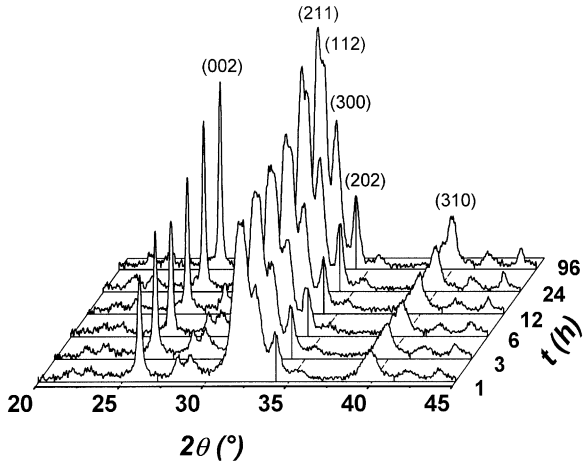

Fig. 3. XRD spectra of the HA nanoparticles synthesised at 80 °C with various ripening times.

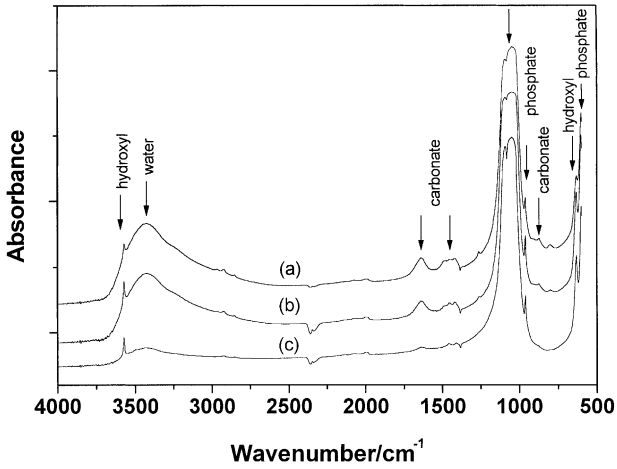

Fig. 4. The normalised FTIR spectra of HA powder synthesised at 80 °C for different ripening times: (a) 1 h, (b) 96 h and (c) after calcination of sample (b).

powders, also decreases with increasing the ripening time. The lower combined water content results from the higher crystallinity of HA powder, implying the crystalline HA powder is less hydrophilic than its amorphous counterpart.

A further evidence for the change of combined water with ripening time was provided by the TG–DTA measurements. As shown in Fig. 5, the weight loss of HA powders heated up to 750 °C is about 7.6 and 6% for 1- and 96-h ripening samples, respectively. The area of endothermic peak on DTA curve shows the same result, too. The weight loss starts at about 100 °C and ends at about 500 °C based on the DTA curves. This weight loss comes from the elimination of combined water.[30] There is also a small endothermic peak at about 480 °C, which may be resulted from the decomposition of ammonium chloride residues. No such small endothermic peak can be distinguished for the calcined sample (curve c).

This crystalline behaviour as a function of ripening time can be explained by the mechanism of crystal growth in solution. It is well known that precipitation of particles involves nucleation and growth from a supersaturated solution. Chemical precipitation often experiences high reaction-induced supersaturation, leading to high nucleation rates. In this case, a crystal nucleus usually has a rough surface due to the rapid production of insoluble materials. This rough surface provides energetically favourable conditions for crystal growth because the molecules adding on it has greater sticking probability.[31] So the rough surface results in high growth rate. However, as the crystal continues to grow, its surface becomes smoother and as a result, the rate of crystal growth slows down. This is because the addition of molecules on the smooth surface has lower sticking probability.[31] Our results shown above are in close agreement with the trend predicted by this mechanism. TEM observations on the morphology changes of the HA as a function of ripening time (Fig. 6) provide further evidence that this mechanism is controlling the rate of crystallisation. These TEM micrographs clearly show that the particles become increasingly regular and smooth with increasing ripening time.

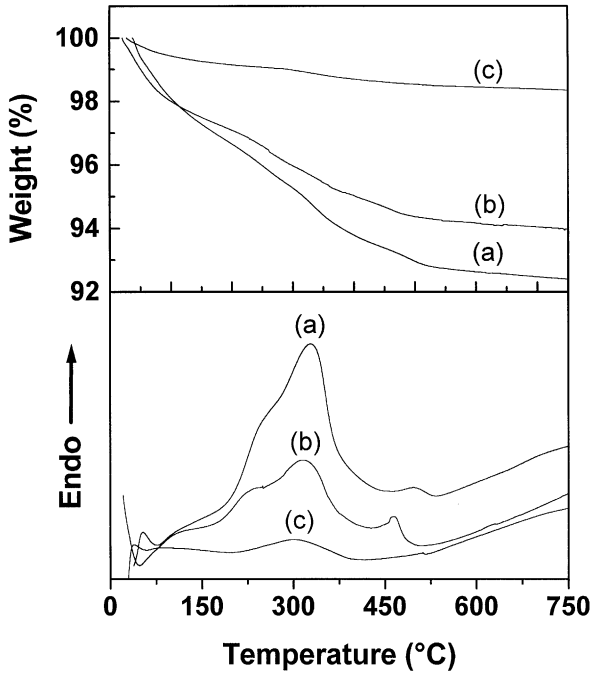

Fig. 5. TG–DTA curves for the same samples as in Fig. 4.

3.3. Effect of calcinations

The influence of calcination on the crystallinity and crystallite size of the HA nanoparticles was also investigated. The XRD diffraction patterns for the HA powders prepared at different temperatures and ripening times after calcination at 650 °C for 6 h are shown in Figs. 7 and 8, respectively. The calcined HA powders show much sharper diffraction peaks and higher crystallinity (X_c), compared with the corresponding "as prepared" ones (Figs. 1 and 3; Tables 1–3). However, it is interesting to notice that the change in crystallite sizes (X_s) after calcination is dependent on the crystallinity and crystallite sizes of "as prepared" HA powders. After calcination, the X_s values increase for the HA powders with lower crystallinity and smaller crystallite sizes but decrease for those with high crystallinity and larger crystallite sizes (Tables 1–3). This unusual change in crystallite size after calcination was also observed by Gibson et al.[29] for the Ca-deficient apatites after heating to temperatures between 650 and 750 °C for 2 h, which was attributed to the loss of water (dehydration) in the Ca-deficient apatites during the phase transformation from Ca-deficient apatites to β-tricalcium phosphate. The water loss was confirmed by FTIR analysis as the disappearance of characteristic peak at 3569 cm^{-1} for the hydroxyl group in the Ca-deficient apatites.[28,29]

As shown in the previous section, the broad peak ranged from 2500 to 3700 cm^{-1} in the FTIR spectra of the our samples (Fig. 4) reflects significant amount of combined water in the samples, especially for the "as prepared" ones. The intensity of this peak decreases very much after calcination, indicating the water loss occurred during calcination. However, the two small sharp peaks at 632 and 3571 cm^{-1}, which are attributed to the hydroxyl group in HA chemical structure, remains after calcination. Furthermore, the XRD results (Fig. 7) show that no new phases are formed after calcination except for HA. These results suggest that no dehydration happens within the HA molecules during calcination and the water loss in the samples is resulted from the loss of combined water in the HA powders. The TG–DTA analyses give the same results. The calcined sample shows much less weight loss com-

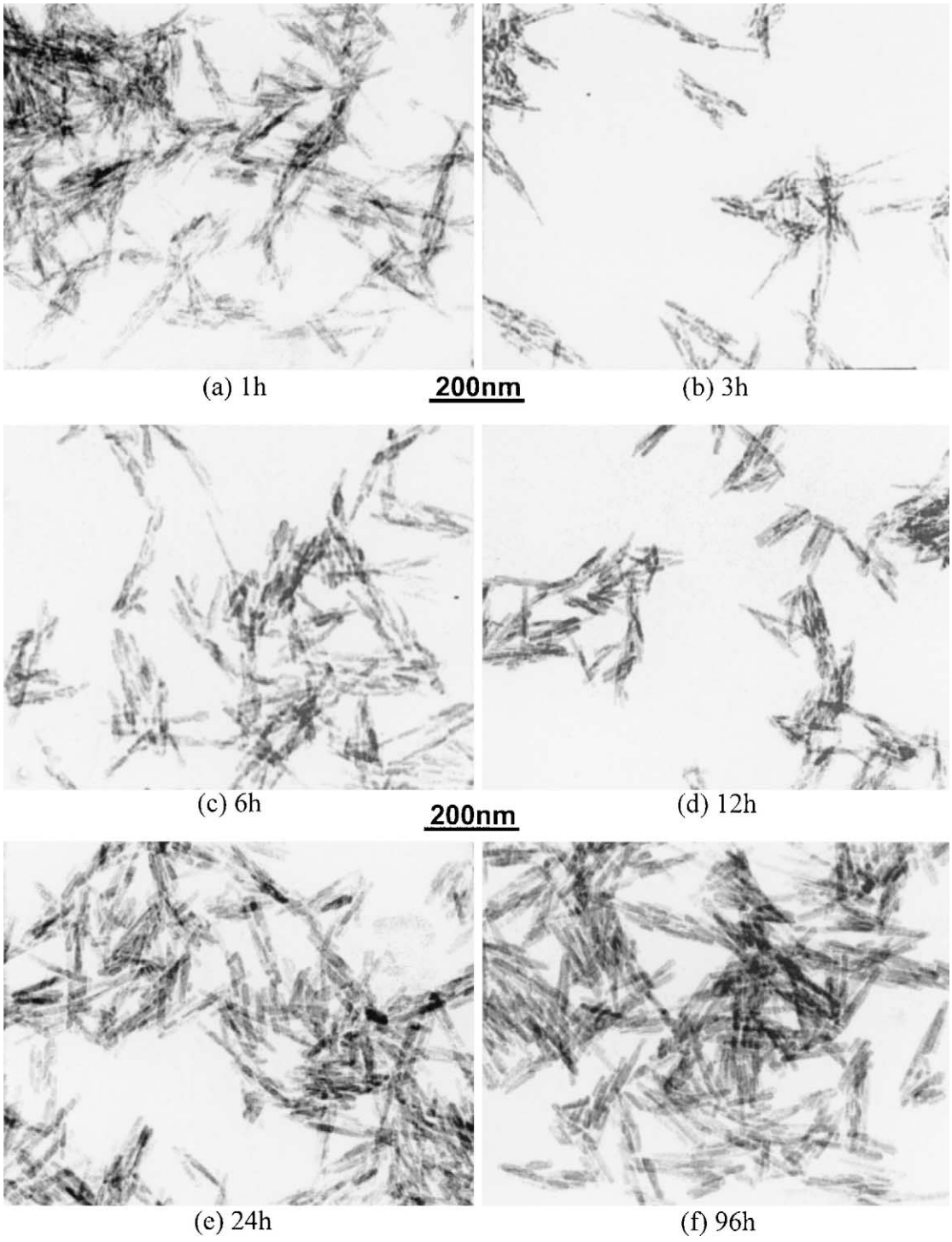

Fig. 6. TEM micrographs of the HA nanoparticles synthesised at 80 °C with various ripening times.

pared to its "as prepared" counterpart (Fig. 5). Therefore, the water loss in the HA powders cannot explain the calcination-induced X_s decrease for some samples in present work.

There are two different crystallisation processes involved in the crystallisation of HA nanoparticles during synthesis and calcination. As discussed in the previous section, the crystallisation of HA during synthesis follows a mechanism of solution crystallisation. Since the crystal growth proceeds through the packing of HA molecules from the solution on the formed nuclei during the ripening process, the crystallites can freely grow on the surfaces of the precipitates in all directions. It is expected that the larger crystallites will be formed with

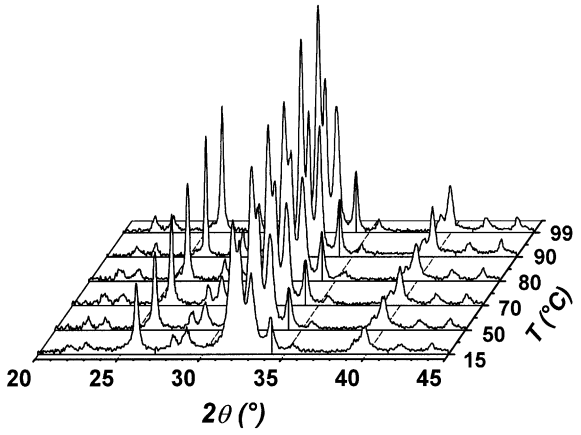

Fig. 7. XRD spectra of the same samples as in Fig. 1 but after calcination at 600 °C for 6 h.

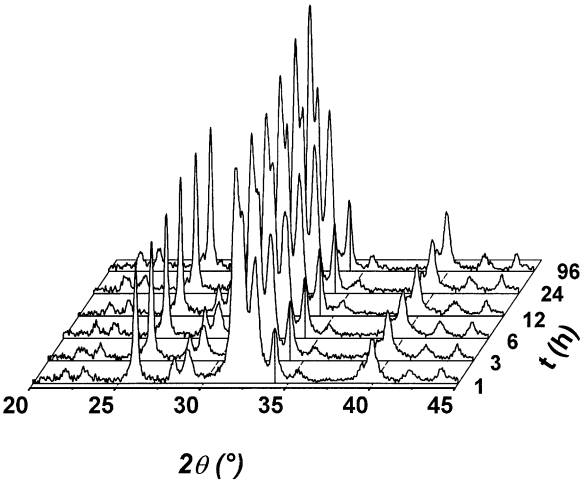

Fig. 8. XRD spectra of the same samples as in Fig. 3 but after calcination at 600 °C for 6 h.

longer ripening time until the crystallisation reaches to its equilibrium. The monotonous increase of X_s with X_c for the "as prepared" samples (Tables 1–3) supports the above hypothesis very well.

On the other hand, during calcination, crystallisation of HA nanoparticles experiences both the nucleation and crystal growth by the rearrangement of HA molecules in amorphous phase. The nucleation and growth take place throughout the precipitates rather than on the surfaces only. As more HA molecules are available inside the precipitates for the nucleation and the crystal growth is in a confined environment, as well as the diffusion of the molecules in solid state is very slow, relatively smaller but more crystallites are expected to be produced in present calcination conditions. The dramatic increase in X_c after calcination indicates that the number of crystallites formed during calcination is large than that formed during synthesis, particularly for the "as prepared" HA powders with lower crystallinity. As a result, the apparent X_s is reduced after calcination for the "as prepared" samples with high crystallinity and larger crystallites because a large amount of relatively smaller new crystallites are formed during calcination. On the other hand, the increased X_s for the "as prepared" samples with lower crystallinity and smaller crystallites comes from the growth of these smaller crystallites and new crystallites formed during calcination, which are relatively larger than "as prepared" smaller crystallites (Tables 1–3).

4. Conclusion

The chemical precipitation through aqueous solutions provides a simple and economic route for synthesis of hydroxyapatite nanoparticles. The crystallinity and morphology of the resulting nanoparticles are dependent on the synthetic temperature and ripening time. The crystallinity and crystallite size of the HA nanoparticles increase with the increase of synthetic temperature and ripening time. The nanoparticles with lower crystallinity show needle-like shape with rough surface and blurred contour and also have higher combined water content, whereas the nanoparticles with higher crystallinity have bar-like shape with smooth surface and clear contour, and the combined water is also lower. Calcination at 650 °C for 6 h leads to significant increase in crystallinity of the HA nanoparticles. The decrease of crystallite size after calcination for the "as prepared" HA nanoparticles with larger crystallites is mainly due to formation of more relatively smaller nanocrystals during calcination rather than the loss of water in the HA molecules.

Acknowledgements

The authors would like to acknowledge the financial support of the Engineering and Physical Sciences Research Council (EPSRC) in UK (GR/N39272/01). Mrs. P.M. King is gratefully acknowledged for her kind help in XRD measurements.

References

1. Doremus, R. H., *J. Mater. Sci.*, 1992, **27**, 285.
2. Nery, E. B., Lynch, K. L., Hirthe, W. M. and Mueller, K. H., *J. Periodotol.*, 1975, **46**, 328.
3. de Groot, K., *Bioceramics of Calcium Phosphate*. CRC Press, 1984.
4. Hench, L. L., *J. Am. Ceram. Soc.*, 1991, **74**, 1487.
5. Kim, W., Zhang, Q. W. and Saito, F., *J. Mater. Sci.*, 2000, **35**, 5401.
6. Tas, A. C., *J. Eur. Ceram. Soc.*, 2000, **20**, 2389.
7. Jarcho, M., Bolen, C. H., Thomas, M. B., Bobick, J., Kay, J. F. and Doremus, R. H., *J. Mater. Sci.*, 1976, **11**, 2027.
8. Lopez-Macipe, A., Rodriguez-Clemente, R., Hidalgo-Lopez, A.,

Arita, I., Garcia-Garduno, M. V., Rivera, E. and Castano, V. M., *J. Mater. Synth. Process*, 1998, **6**, 121.
9. Huang, L. Y., Xu, K. W. and Lu, J., *J. Mater. Sci. Mater. Med.*, 2000, **11**, 667.
10. Weng, W. J. and Baptista, J. L., *Biomaterials*, 1998, **19**, 125.
11. Weng, W. J. and Baptista, J. L., *J. Mater. Sci. Mater. Med.*, 1998, **9**, 159.
12. Katsuki, H., Furuta, S. and Komarneni, S., *J. Am. Ceram. Soc.*, 1999, **82**, 2257.
13. Yoshmura, M., Suda, H., Okmoto, K. and Loku, K., *J. Mater. Sci.*, 1994, **29**, 3399.
14. Lim, G. K., Wang, J., Ng, S. C. and Gan, L. M., *Langmuir*, 1999, **15**, 7472.
15. Lim, G. K., Wang, J., Ng, S. C. and Gan, L. M., *J. Mater. Chem.*, 1999, **9**, 1635.
16. Shai, D. L. and Jiang, G. W., *Mater. Sci. Eng.*, 1998, **C6**, 175.
17. Fujishiro, Y., Nishino, M., Sugimori, A., Okuwaki, A. and Sato, T., *J. Mater. Sci. Mater. Med.*, 2001, **12**, 333.
18. Lin, F. H., Lin, C. C., Liu, H. C., Huang, Y. Y., Wang, C. Y. and Lu, L. M., *Biomaterials*, 1994, **15**, 1087.
19. Luo, P. and Nieh, T. G., *Biomaterials*, 1996, **17**, 1959.
20. Khor, K. A., Chang, P. and Wang, Y., *J. Thermal. Spray Technol.*, 1998, **7**, 254.
21. Fujishiro, Y., Yabuki, H., Kawamura, K., Sato, T. and Okuwaki, A., *J. Chem. Technol. Biotechnol.*, 1993, **57**, 349.
22. Bouyer, E., Gitzhofer, F. and Boulos, M. I., *J. Mater. Sci. Mater. Med.*, 2000, **11**, 523.
23. Bernard, L., Freche, M., Lacout, J. L. and Biscans, B., *Powder Technol.*, 1999, **103**, 19.
24. Wang, M., Joseph, R. and Bonfield, W., *Biomaterials*, 1998, **19**, 2357.
25. Landi, E., Tampieri, A., Celotti, G. and Sprio, S., *J. Eur. Ceram. Soc.*, 2000, **20**, 2377.
26. PDF Card No 9-432, ICDD, Newtown Square, Pennsylvania, USA.
27. Jenkins, R. and Snyder, R. L., *Introduction to X-ray Powder Diffractometry*. John Wiley & Sons, New York, 1996.
28. Yubao, L., Klein, C. P. A. T., de Wijn, J., van de Meer, S. and de Groot, K., *J. Mater. Sci. Mater. Med.*, 1994, **5**, 263.
29. Gibson, I. R., Rehman, I., Best, S. M. and Bonfield, W., *J. Mater. Sci. Mater. Med.*, 2000, **11**, 799.
30. Tampieri, A., Celotti, G., Sprio, S. and Mingazzini, C., *Mater. Chem. Phys.*, 2000, **64**, 54.
31. Ring, T. A., *Fundamentals of Ceramic Powder Processing and Synthesis*. Academic Press, San Diego, 1996 (Chapter 6).